EFFECT OF RIFLING GROOVES ON THE PERFORMANCE OF SMALL-CALIBER AMMUNITION

Sidra I. Silton* and Paul Weinacht
US Army Research Laboratory
Aberdeen Proving Ground, MD 21005-5066

ABSTRACT

A combined experimental and computational investigation was performed to examine the effect of rifling grooves on the aerodynamics of projectiles and determine whether the aerodynamics associated with the rifling grooves are a potential mechanism for in-flight trim angles. The experimental program consisted of spark-range firings of bullets from the standard twist barrel spanning the range of velocities typically encountered in flight. Additionally, sabot-launched smooth and pre-engraved bullets were fired from over-sized barrels with twist rates to match in-flight spin rates and velocities. The computational technique was first validated using existing wind tunnel data for a rifled projectile. Computational results were then obtained to complement the results from the spark-range testing. The results show that the aerodynamic components most sensitive to the rifling grooves are the Magnus force and moment and the roll-damping moment. These effects are relatively small for typical in-flight conditions and are unlikely to produce trim angle effects and can be ignored in future computational and experimental efforts.

1. INTRODUCTION

Many gun-launch munitions require spin stabilization. Spin stabilization typically utilizes rifling grooves within the gun tube to impart the desired spin rate to the projectile as it traverses the gun tube. For small caliber munitions, the rifling grooves engage the projectile body itself. The rifling process "engraves" rifling grooves in the projectile body slightly modifying the pre-launch projectile geometry. It has been suspected that the rifling grooves can affect the aerodynamics of the projectile.

One reason the rifling grooves have been suspected to affect the aerodynamics is that the projectile attains an "over-spun" condition as it flies downrange. When fired from a stationary gun, the flow near the grooves is essentially parallel to the grooves as a result of the no-slip boundary condition (Fig. 1). As the projectile flies downrange, the forward velocity slows faster than the spin rate, such that the non-dimensional spin rate (pD/V) increases. This causes the flow near the grooves to no longer be aligned with the grooves (Fig. 1), producing the "over-spun" state. The over-spun condition may result in a change in the aerodynamic characteristics of the projectile. The projectile can also achieve an "under-spun" state when launched from a forward moving gun.

Properly addressing the effect of rifling grooves in both experiments and computations presents a number of challenges and are typically either not completely addressed or ignored. Range experiments for determining the aerodynamics of a projectile at its downrange velocities have typically been accomplished by downloading the propellant charge and shooting the projectile out of its "standard" barrel (McCoy, 1985; McCoy, 1990). This affects the results of the experiment in two ways. First, the spin rate for reduced velocity firings does not match the corresponding spin attained at that velocity in free-flight. Second, the bullet may no longer have the same depth engraving because in-bore pressures produced by the decreased charge weight for downloaded charges are reduced. From a computational perspective, the addition of the grooves presents an additional geometric feature and flow physics that must be resolved, thus increasing the complexity and computational cost of the simulation. To date, Computational Fluid Dynamics (CFD) simulations have assumed a pristine (unengraved) bullet model (Sahu, 1986; Weinact et al., 1986).

The current research effort examines the effect of rifling grooves and spin on the aerodynamics of small caliber munitions both experimentally and computationally. Existing wind tunnel data for a generic grooved projectile was used validate the computational approach. Subsequently, an experimental program consisting of firings in a spark-range aerodynamic facility was executed in parallel with computations to assess the effect of rifling grooves and spin on the projectile aerodynamics.

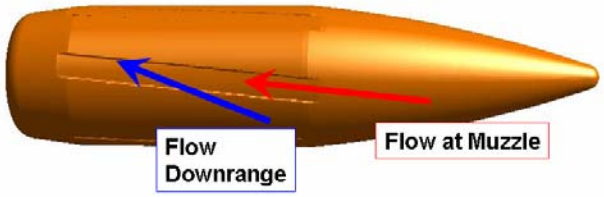

Figure 1. Schematic illustrating over-spun condition for a rifled projectile.

Report Documentation Page

Form Approved
OMB No. 0704-0188

1. REPORT DATE	2. REPORT TYPE	3. DATES COVERED
DEC 2008	**N/A**	**-**

4. TITLE AND SUBTITLE	5a. CONTRACT NUMBER
Effect Of Rifling Grooves On The Performance Of Small-Caliber Ammunition	5b. GRANT NUMBER
	5c. PROGRAM ELEMENT NUMBER
6. AUTHOR(S)	5d. PROJECT NUMBER
	5e. TASK NUMBER
	5f. WORK UNIT NUMBER
7. PERFORMING ORGANIZATION NAME(S) AND ADDRESS(ES) **U. S. Army Research Laboratory Aberdeen Proving Ground, MD 21005-5066**	8. PERFORMING ORGANIZATION REPORT NUMBER
9. SPONSORING/MONITORING AGENCY NAME(S) AND ADDRESS(ES)	10. SPONSOR/MONITOR'S ACRONYM(S)
	11. SPONSOR/MONITOR'S REPORT NUMBER(S)

12. DISTRIBUTION/AVAILABILITY STATEMENT
Approved for public release, distribution unlimited

13. SUPPLEMENTARY NOTES
See also ADM002187. Proceedings of the Army Science Conference (26th) Held in Orlando, Florida on 1-4 December 2008, The original document contains color images.

14. ABSTRACT

15. SUBJECT TERMS

16. SECURITY CLASSIFICATION OF:			17. LIMITATION OF ABSTRACT	18. NUMBER OF PAGES	19a. NAME OF RESPONSIBLE PERSON
a. REPORT	b. ABSTRACT	c. THIS PAGE			
unclassified	**unclassified**	**unclassified**	**UU**	**8**	

2. COMPUTATIONAL APPROACH

Computational methods were used to address the effect of the rifling grooves on the projectile aerodynamics using an overset grid approach (Renze et al., 1992; Meakin, 1991) that utilizes a conformal near-body grid system and an outer off-body Cartesian-based grid system. The near-body grid system contains inter-connecting grids which conform to various parts of the body. The outer, off-body Cartesian grid system encompasses the near-body grid system and extends to the outer boundary of the computational domain (Fig. 2). The inter-grid connectivity of the overlapping near-body and off-body grids is established using a Chimera overset gridding approach (Chan, 2002). The near-body grid system encompassed 87% of the 5.6 million points used for the complete grid.

Solution of the compressible Reynolds-averaged Navier-Stokes equations was accomplished using the NASA code, Overflow2. The current computations use a three-factor diagonal-implicit, first-order accurate time-stepping scheme that employs second-order accurate central differencing in space. The Baldwin-Barth one-equation turbulence model (Baldwin and Barth, 1991) has been utilized. Characteristics based inflow/outflow boundary conditions have been applied on the boundaries of the domain. On the body surface, no-slip, adiabatic boundary conditions are imposed.

One set of numerical computations is performed at a fixed angle of attack, α, and spin rate in order to obtain the static aerodynamic coefficients, as well as the roll damping ($\alpha = 0°$) and Magnus moment ($\alpha = 2°, 5°$) coefficients. The combined spin and angle of attack for axisymmetric bodies can be addressed with a steady-state approach by applying a simple tangential velocity boundary condition to the body surface. However, the combination of non-axisymmetric body rotation and angle of attack produces a time-dependent flow field that requires the application of a time-accurate approach. The time-dependent computations were accomplished using a body-fixed, rotating near-body mesh that rotates relative to the stationary outer off-body Cartesian grid system. It was determined that inner iterations at each time step were required to obtain a suitably converged solution for the spin-dependent aerodynamic coefficients such as Magnus moment and roll-damping moment coefficients. For the smooth body geometry, the time-accurate results can be compared to the steady results to determine the required time step and inner iterations. The study also showed that 5000-7000 physical time steps, with 20 inner iterations were required to obtain the steady-state spinning solution from the initial converged non-spinning solution. This corresponds to the time required for a fluid particle to travel one to two body lengths in the free stream. Studies of the effect of inner iterations were also performed for the grooved projectile body and similar results were found.

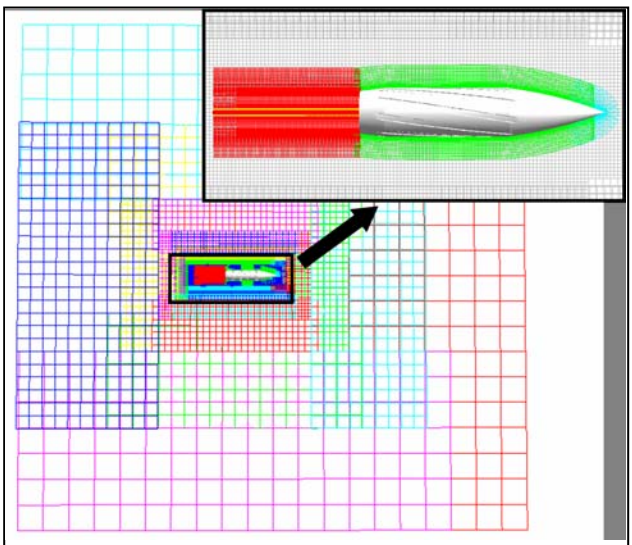

Figure 2. Overset grid utilizing a conformal near-body grid system (inset) and an outer off-body Cartesian-based grid system.

A second set of numerical experiments are required to obtain the pitch-damping coefficients associated with the aerodynamics produced by the non-zero angular rates. At least two approaches for performing the pitch damping experiment currently exist which rely on imposed motions to provide the angular rates necessary to produce the forces and moments associated with the pitch-damping coefficients. The approach presented here employs an imposed coning motion to produce the pitch-damping force and moment, which can be directly obtained from the computed side force and moment normalized by the angle of attack and coning rate (Schiff, 1972; Weinacht, 1997; DeSpirito et al., 2008). Depending on the geometry and type of coning motion selected, this computation can be performed as a steady-state computation

Global integrated force/moment data was obtained from the computed flow fields using the FOMOCO utility (Chan and Buning, 1996). Force and moment distributions along the body were also obtained from the computed flow fields through minor modifications to the existing code and additional auxiliary post-processing tools.

3. EXPERIMENTAL APPROACH

The experimental investigation of the effect of rifling grooves was performed in the ARL Aerodynamics Experimental Facility. This spark range facility is designed to evaluate the complete aeroballistics of projectiles as described by Braun (Braun, 1958). The range facility consists of 39 orthogonal spark shadowgraph stations (Fig. 3) over 100-m of trajectory length with the first station located approximately 1.8 m downrange of the muzzle. Infrared sensors detect the passage of the projectile through the stations and a

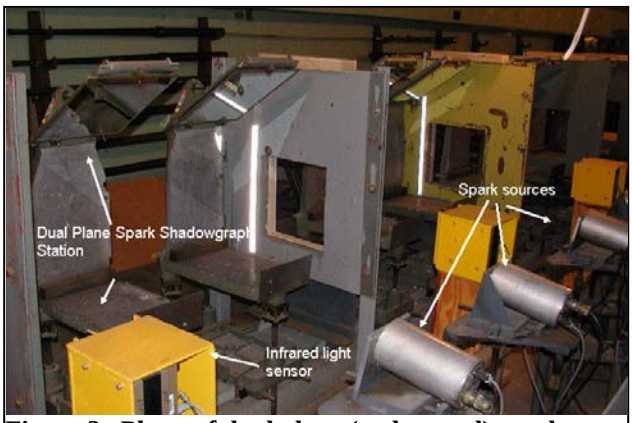

Figure 3. Photo of dual plane (orthogonal) spark shadowgraph stations with infrared sensor triggers and spark source.

computer system triggers the spark sources that project a vertical and horizontal direct shadow image of the passing projectile on the film and records the spark time. The stations are surveyed into a fiducial system that is simultaneously imaged on the film with the projectile. The film is processed after each shot and read using a precision light table to produce the raw experimental data (range, deflection, altitude, pitch, yaw, and roll) relative to the earth fixed range coordinate system, as a function of the spark time. By processing the raw data using a standard linear theory analysis and a 6-DOF numerical integration technique integrated in ARFDAS (ArrowTech Associates, 1997), a complete set of coefficients can be obtained.

In order to conduct the experimental investigation of the effect of rifling grooves and spin on a small-caliber projectile (specifically, 5.56 mm), both pristine and grooved projectiles were used (Fig. 4). Constant spin, grooved projectiles were fired from an M16A2 barrel using a variable propellant charge weight to attain the desired velocity. These firings are representative of the typical approach used to characterize the aerodynamics of small-caliber bullets. To obtain a spin rate that corresponds to the downrange velocity, a second set of projectiles was fired from the M16A2 barrel using the standard propellant charge weight and recovered from a gel block at 600m (pre-engraved). The pre-engraved projectiles were then sabot-launched from the appropriate high twist, over-sized Mann barrels (7.62mm). Though representative of in-flight conditions, this approach required considerably more effort than the typical approach. A third configuration, consisting of pristine bullets that were sabot launched from the over-sized barrels in the same manner at the second configuration.

Figure 4. Pristine (left) and pre-engraved (right) 5.56 mm projectiles

4. RESULTS

4.1 Numerical Validation

The assessment of the effect of rifling grooves and spin rate has been made using results from existing wind tunnel tests and recently performed aeroballistic spark range testing. In each case, the experimental results were augmented with computational fluid dynamics predictions.

Computational predictions were made for the wind tunnel model shown in Fig. 5 in order to validate the methodology. The diameter of the wind tunnel model was 51 mm. to allow testing at a Reynolds number equivalent to a 20 mm projectile at free flight atmospheric conditions. The rifling grooves were equivalent to those for the 20 mm rifling and consisted of nine grooves, 0.115 calibers wide and 0.0205 calibers deep with a twist rate of 1 turn in 20 calibers of travel. Wind tunnel tests were also performed on a smooth (ungrooved) version of the model. Computations were performed at Mach 2.0 for a Reynolds number based on diameter of 9×10^5 for both the smooth and grooved models over a range of non-dimensional spin rates from 0 to 0.4.

The aerodynamic forces and moments were compared for both smooth and grooved models. For many of the static aerodynamic coefficients, little effect of the grooves was noted. For the drag coefficient, the differences were less than 0.6%. For the normal force and pitching moment coefficients, the differences were less than 1.0% and 2.5% respectively. Both the predictions and the wind tunnel results showed a slight decrease in the pitching moment when the grooves were present. For the grooved body, the predictions indicated a slight decrease (2%) in the pitching moment as the non-dimensional spin rate was increased from 0 to 0.4. The predicted pitching moments for the grooved body were

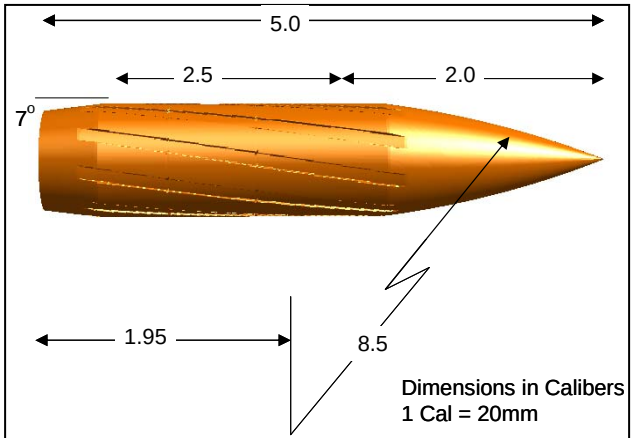

Figure 5. Geometric features of the boattailed Army-Navy spinner rocket.

within ±1% of the single pitching moment coefficient reported from the wind tunnel test. More significant differences were noted for the Magnus (side) force and moment and the roll damping moment.

The roll moment and Magnus force and moment for the grooved projectile exhibited the classical linear variation with spin rate characteristic of smooth projectiles, except the grooved projectile exhibited non-zero force or moment at zero-spin rate due to the non-axisymmetric nature of the rifling grooves. Most trajectory simulations and data reduction procedures assume no zero-spin offset in these coefficients. Therefore, one approach for obtaining the roll-damping moment and the Magnus force and moment is to normalize the force or moment by the spin rate to obtain an "effective" coefficient that is dependent on spin rate. Because the spin rate changes relatively slowly in flight and can be related directly related to the local Mach number, the "effective" Magnus, although spin-dependent, can be treated as a function of Mach number.

Excellent agreement between the computed and wind tunnel measurements of the effective Magnus moment is shown in Fig. 6. The relatively small differences between the computed Magnus moments at 2.2 and 4.3 degrees indicate that the Magnus moment coefficient is relatively independent of angle of attack (at least for small angles) and can be represented as a constant for a fixed spin rate. The results do show a dependence of the Magnus moment on spin rate, particularly for low spin rates. At higher spin rates, the Magnus moment becomes relatively constant as the effect of the zero-spin offset is diminished. As mentioned previously, the non-dimensional spin rate will typically increase during flight because the forward velocity of the projectile decreases faster than the dimensional spin rate. Increases in the non-dimensional spin rate beyond the non-dimensional launch spin rate of 0.314 are seen to produce relatively small changes in the Magnus moment (and dynamic stability) due to the grooves.

Figure 7 shows the effective roll-damping coefficient for the ANSR body at 2.2 and 4.3 degrees angle of attack. At the launch spin rate (0.314), the effective roll-damping for the grooved body is nearly 25% higher than for the smooth body. The effective roll-damping of the grooved body is seen to increase relative to that of the smooth body as the projectile becomes over-spun. For the under-spun condition, much larger variations in the effective roll-damping are possible, although this is unexpected for typical launch conditions.

4.2 Current generation 5.56mm ammunition

The validated computational technique and a spark range test were used to examine the effect of rifling grooves on current generation 5.56mm ammunition typically fired from the M16A2 rifle. Three configurations of the M193 projectile (Fig. 8) are consider for this portion of the study; grooved (pre-engraved) body at a constant twist rate corresponding to pD/V = 0.2 and at in-flight pD/V and smooth body at the in-flight pD/V. The spark range tests were conducted at Mach 2.6, 2.1, 1.6 and 1.1 over a range of angles of attack to obtain a complete set of static coefficients and dynamics derivatives. The computations were completed for Mach

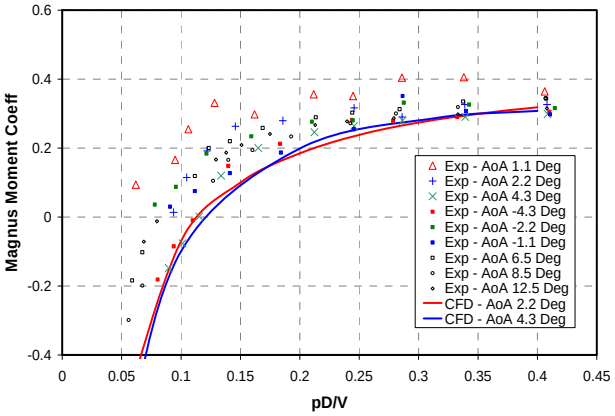

Figure 6. Comparison of computed Magnus moment coefficient versus spin rate with wind tunnel data for boattailed ANSR configuration.

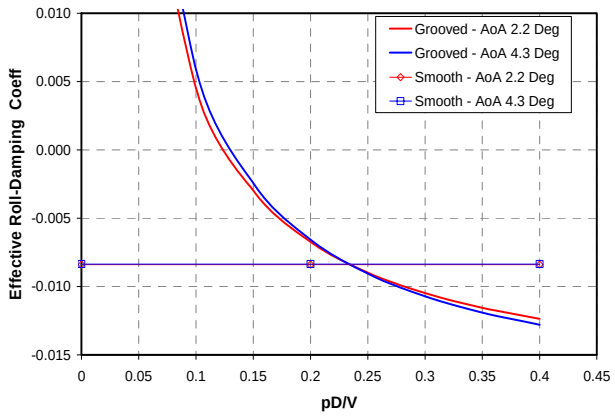

Figure 7. Comparison of the computed effective roll-damping moment coefficient versus spin rate for grooved and smooth boattailed ANSR configuration.

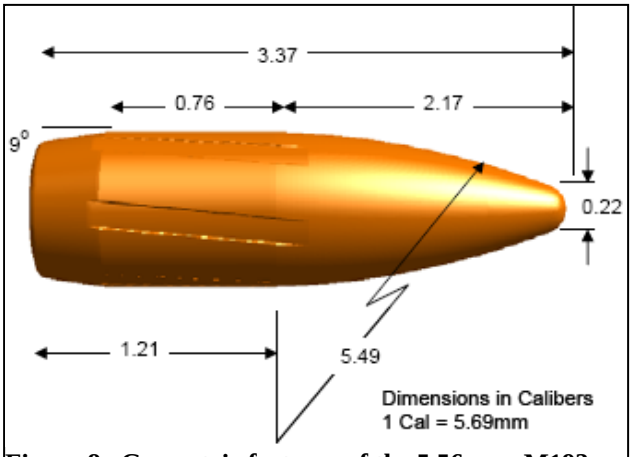

Figure 8. Geometric features of the 5.56-mm M193.

2.5 and 1.35 at two degrees angle of attack at standard atmospheric conditions. The rifling on the computational geometry was modeled as six grooves that are 0.18 calibers wide and 0.01 calibers deep with the twist rate of the M16A2 barrel. Additional CFD simulations were completed on the smooth body model over a larger range over Mach numbers for additional comparison to the experimental results.

Similar to the wind tunnel model, very little difference in most of the aerodynamic coefficients was seen between configurations indicating that neither spin rate nor engraving has a significant effect for either the experimental or computational results, especially the static coefficients. Figure 9 shows the prediction of the zero-yaw axial force coefficient. The range data shows no significant differentiation between configurations noticeable. The agreement with computational results is quite good. Note that while the Magnus computations were performed at $\alpha = 0°$, the coning computations were completed at $\alpha = 2°$. The differences of 1-2% are attributable to the quadratic yaw drag. The normal force and pitching moment coefficients are shown in figures 10 and 11. While only the results of the smooth body computational model shown, all the range data is included. The agreement between the range configurations as well as the coning (zero-spin rate) and Magnus (zero-angular rate) computations demonstrate the insensitivity of both of these coefficients to spin and angular rate. Again, the most significant differences were again seen in the Magnus moment and the roll-damping moment.

The dynamic derivatives were not quite as straight forward in dismissing the effects of spin rate of engraving. The effect of either on the pitch-damping moment coefficient appears to be minimal (Fig. 12). A comparison of the spark range and computed measurements of the effective Magnus moment coefficient is shown in Fig. 12. There is a large amount of scatter within the experimental data, but it does not correlate to either spin rate or engraving. It is within the accuracy of the range measurement which can be as large as 25-30%. The computational results follow the trend of the experimental data well within this accuracy.

A comparison of the spark range and computed measurement of the effective Magnus moment coefficient is shown in Fig. 13. The spark range results have a large amount of experimental error, especially as the Magnus moment coefficient approaches zero. Although the range data and the computational results do not perfectly agree, the trends are definitely similar. At near launch velocity, the range data and the computations indicate no difference, which is to be expected as the flow is aligned with the grooves. As the velocity decreases, the spark range data shows that the constant-twist projectile has lower coefficient values than the other two configurations. At the lowest Mach number, the computations and the range data both indicate that the grooved projectile with in-flight pD/V has a slightly higher Magnus moment coefficient. The observed differences at this lowest Mach number are very small considering the projectile is the most over-spun. In fact, the differences between configurations in the experimental results are barely outside the measurement error. Thus, the variations in the computational results are also not viewed as particularly significant.

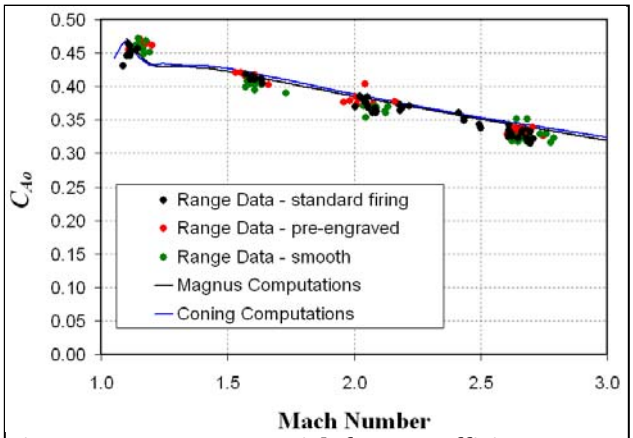

Figure 9. Zero-yaw axial force coefficient versus Mach number, M193.

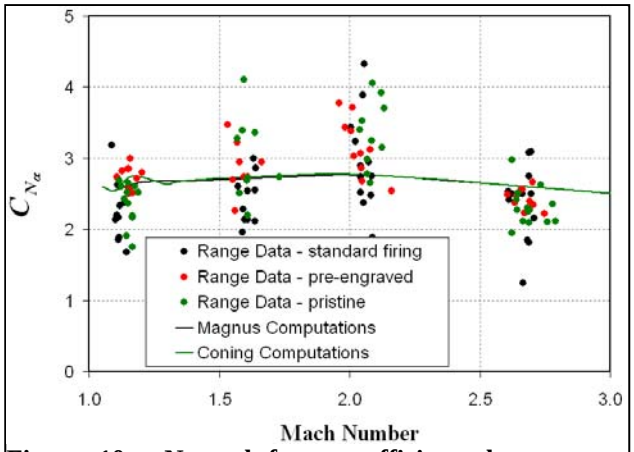

Figure 10. Normal force coefficient slope versus Mach number, M193.

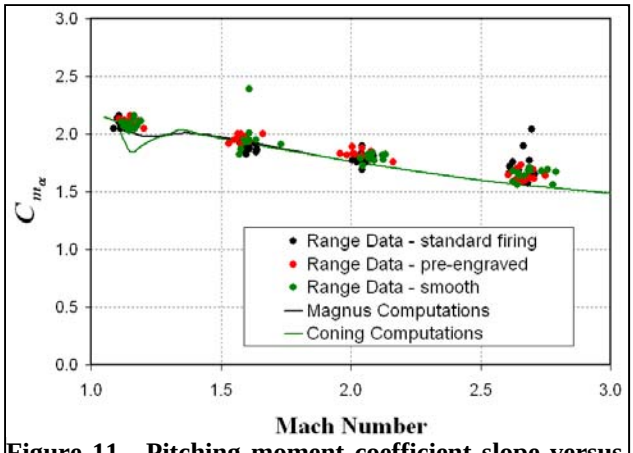

Figure 11. Pitching moment coefficient slope versus Mach number, M193.

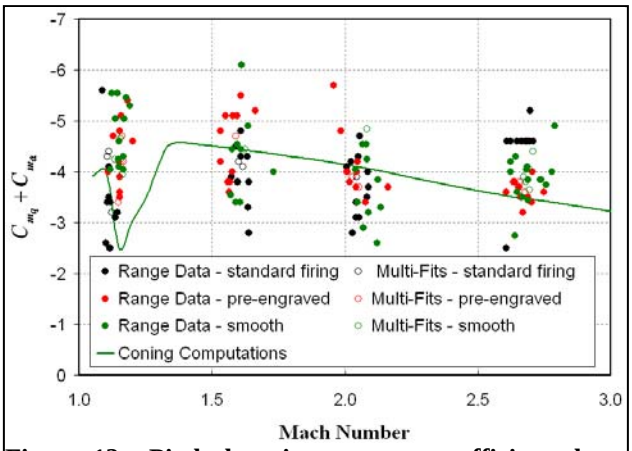

Figure 12. Pitch-damping moment coefficient slope versus Mach number, M193.

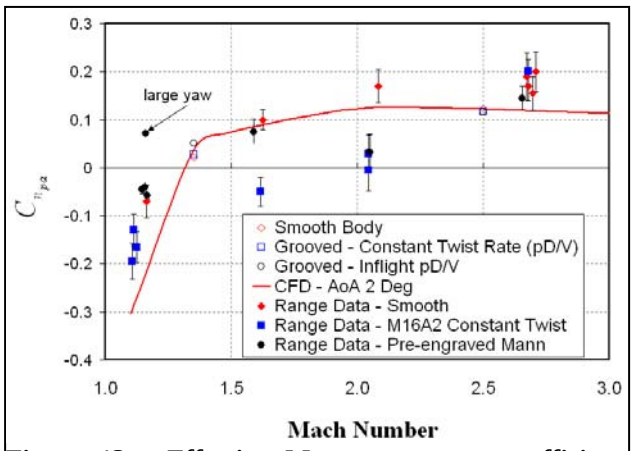

Figure 13. Effective Magnus moment coefficient versus Mach number, M193.

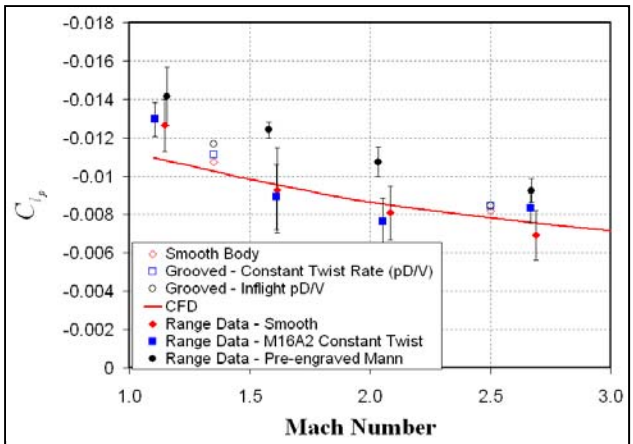

Figure 14. Effective roll-damping coefficient versus Mach number, M193.

Figure 14 shows the effective roll-damping coefficient for the M193 con-figurations investigated. The error bars on the spark range data represent one standard deviation from the mean roll-damping coefficient. At (near) launch velocity the range data and the computational results show a slightly lower roll-damping coefficient for the smooth body configuration. Within the error of the ballistic testing, the variations are not significant. At the next two lower Mach numbers, the range data shows the pre-engraved projectile at in-flight pD/V to have a measurably larger effective roll-damping coefficient. At the lowest Mach number, however, the differences are again within the error of the experimental data. The computational results confirm that the grooved body at in-flight pD/V has a slightly higher roll-damping coefficient at the lower Mach number, but this is not considered significant due to the variation of the experimental data.

4.3 Dynamic stability and trim angle

Using the aerodynamic characterization (computational or experimental) completed as part of this study the stability, performance and 6 degree-of-freedom trajectory of the projectile can be assessed for each configuration. As the aerodynamic coefficients were not found to vary significantly between configurations, the trajectory of the round would not be affected by the configuration tested. However, both stability and performance, as gauged by the trim angle, could be affected by the configuration chosen. Specifically, a constant twist rate or the inflight twist rate as the stability of the round is dependent on the spin rate.

In order for a spin-stabilized projectile to have a stable flight, the round must remain both gyroscopically and dynamically stable throughout it flight trajectory. In order for a round to be gyroscopically stable, the gyroscopic stability factor, S_g, given by equation (1) must be greater than one.

$$S_g = \frac{I_x p^2}{2\rho I_x S d V^2 C_{m_\alpha}} \tag{1}$$

Assuming that the round is gyroscopically, the dynamic stability of the round can then be assessed. The dynamic stability factor, S_d, is given by

$$S_d = \frac{2\left(C_{L_\alpha} + k_x^{-2} C_{n_{p\alpha}}\right)}{C_{L_\alpha} - C_D - k_y^{-2}\left(C_{m_q} + C_{m_{\dot{\alpha}}}\right)} \tag{2}$$

where ρ is the free stream density, d is the projectile diameter, S is the projectile reference area, V is the free stream velocity, and I_x is the axial moment of inertia. Additionally,

$$k_x^{-2} = \frac{md^2}{I_x}, \quad k_y^{-2} = \frac{md^2}{I_y} \tag{3}$$

Where m is the projectile mass and I_y is the transverse moment of inertia. Note that all of the aerodynamic coefficients in equations (1) and (2) are multiplied by

$$\frac{\rho S d}{2m} \tag{4}$$

Additionally, the projectile must remain within the dynamic stability bound as defined by

$$\frac{1}{S_g} < S_d\left(2 - S_d\right) \tag{5}$$

Fig. 15 shows a plot of the inverse of the gyroscopic stability factor versus the dynamic stability for the standard firing (constant pd/V) and pre-engraved (in-flight pd/V) configurations with the dynamic stability bound, $\frac{1}{S_g} = S_d\left(2 - S_d\right)$, overlaid. Also included in Fig. 15 is the standard firing configuration adjusted for in-flight pd/V. The range data shows that the projectile is gyroscopically stable at all velocities. As expected, S_g of the pre-engraved rounds and the adjusted spin rounds are consistent with the standard firing having a larger S_g due to a larger spin rate. The projectile is also dynamically stable for Mach numbers greater than Mach 1.5. Near Mach 1.1, the dynamic stability of the round appears to depend on which configuration is being analyzed as well as the angle of attack. The dynamic stability of the pre-engraved rounds is significantly increased and all pre-engraved rounds at Mach 1.1 are stable. The dynamic instability indicates that a small yaw limit cycle may occur. A small yaw limit cycle was in fact present for the Mach 1.1 standard firing configuration (approximately 2°). The increased dynamic stability of the pre-engraved rounds is due to this configuration having a larger (less negative) Magnus moment coefficient than the standard firing configuration. This can partially be attributed to the pre-engraved round having higher yaw levels ($1.5° < \alpha < 8°$) than the standard firing round ($0.3° < \alpha < 4°$). However, based on the adjusted spin standard firing stability, the lowest yaw pre-engraved rounds would be expected to be unstable. Additional low yaw shots (below 2°) of the pre-engraved configuration would be necessary to more accurately determine the limit cycle.

The stability factors have also been computed for the computational smooth body from Mach 1.1 to 3 at the inflight spin rate (coefficients determined at a constant pd/V). The predictions show that the projectile is gyroscopically stable ($s_g > 1$) at all velocities. Comparing these results to those of the standard firing, adjusted spin, shows that the rifling grooves have minimal effect. As with the engraved projectile, the smooth projectile remains dynamically stable across the Mach number regime except near Mach 1.1 to Mach 1.2 at low angles of attack indicating a small yaw limit cycle is likely. The agreement between the computational smooth body results and the experimental standard firing results increase the confidence of the authors for using either or these methods in the future.

5. CONCLUSIONS

A sophisticated computational technique has been applied to examine the effect of rifling and spin rate on the aerodynamic characteristics of small caliber ammunition. The computational approach has been validated by comparison with wind tunnel data for a generic projectile geometry with rifling grooves at Mach 2. The computational show the relative effect between smooth and grooved (rifled) projectiles to be minimal over a range of spin rates and that the rifling grooves do not produce aerodynamic effects responsible for the observed trim angles.. The technique was then applied to a current generation small-caliber projectile. In conjunction with a spark range test, the effect of the rifling grooves and spin rate (constant twist versus inflight pD/V) at both launch and downrange velocities on the aerodynamic coefficients and derivatives were found to either be minimal or within the experimental error of the ballistics testing.

The results have important implications for both CFD and aeroballistic testing of small caliber munitions. An extraordinary amount of additional computational and experimental resources were required to obtain a projectile with proper engraving at a spin rate that

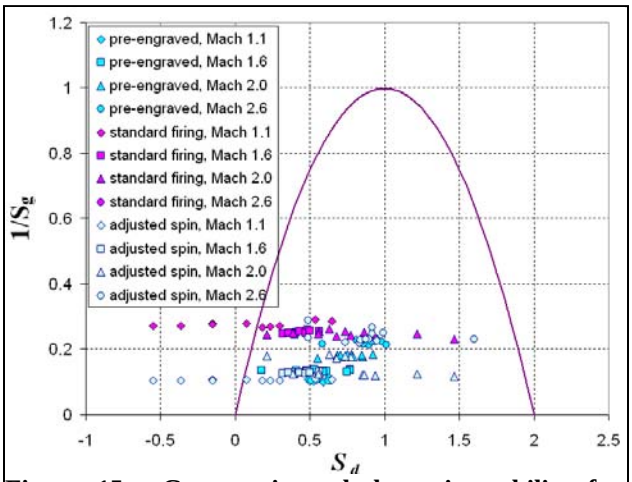

Figure 15. Gyroscopic and dynamic stability for M193 experimental data at muzzle and in-flight spin rates.

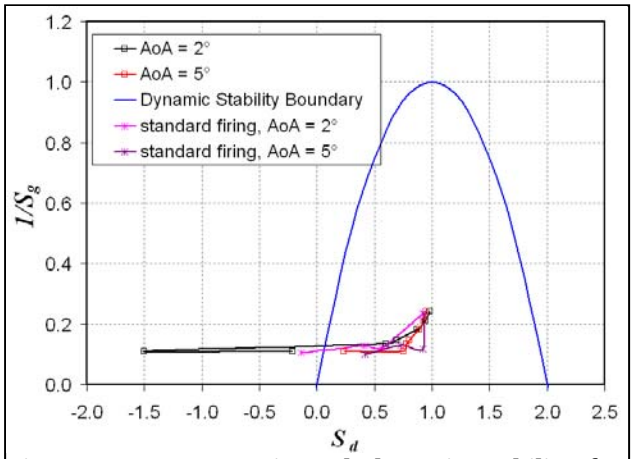

Figure 15. Gyroscopic and dynamic stability for M193 at in-flight spin rates.

corresponds to the Mach number being investigated. Fortunately, the current results indicate that the effect of rifling grooves and spin rate is not particularly important to the determination of the aerodynamic coefficients and dynamic derivatives, so typical CFD and experimental methods can continue to be used. However, if the stability of the round is to be correctly determined for the downrange velocities, the use of the in-flight spin rate is necessary. If only the muzzle spin rates are used, the predicted level of the dynamic instability, manifested as trim angle, will likely be greater than in actuality.

ACKNOWLDGEMENTS

The author wishes to acknowledge the US Army PM-MAS for funding and supporting significant portions of this effort. This work was also supported by a grant of computer time from the Department of Defense High Performance Computing Major Shared Resource Center at the U.S. Army Research Laboratory.

REFERENCES

Arrow Tech Associates, "ARFDAS: Ballistic Range Data Analysis System," User and Technical Manual, South Burlington, VT, May 1997.

Baldwin, B.S. and Barth, T.J., "A One-Equation Turbulence Transport Model for High Reynolds Number Wall-Bounded Flows," AIAA-91-610, January 1991.

Braun, W.F., "The Free Flight Aerodynamics Range," BRL-R-1048, U.S. Army Ballistic Research Laboratory, Aberdeen Proving Ground, MD, July 1958.

Chan, W.M., "The Overgrid Interface for Computational Simulations on Overset Grids," AIAA-2002-3188, June 2002.

Chan, W.M. and Buning, P.G., "User's Manual for FOMOCO Utilities – Force and Moment Computation Tools for Overset Grids," NASA-TM-110408, July 1996.

DeSpirito, J., Silton, S.I., and Weinacht, P., "Navier-Stokes Predictions of Dynamic Stability Derivatives: Evaluation of Steady State Methods," AIAA-2008-0214, Jan. 2008.

McCoy, R.L., "Aerodynamic Characteristics of Caliber .22 Long Rifle MATCH Ammunition, BRL-MR-3877, Ballistic Research Laboratories, Aberdeen Proving Ground, MD, Nov 1990.

McCoy, R.L., "Aerodynamic and Flight Dynamic Characteristics of the NEW Family of 5.56MM NATO Ammunition," BRL-MR-3476, Ballistic Research Laboratories, Aberdeen Proving Ground, MD, Oct 1985.

Meakin, R.L., "A New Method for Establishing Inter-grid Communication Among Systems of Overset Grids", AIAA Paper AIAA-91-1586, June 1991.

Renze, K.J, Buning, P.G., and Ragagopalan, R.G., "A Comparative Study of Turbulence Models for Overset Grids", AIAA Paper AIAA-92-0437, January 1992.

Sahu, J.,"Three Dimensional Base Flow Calculation for a Projectile at Transonic Velocity," AIAA-86-1051, May 1986.

Shiff, L.B., "Nonlinear Aerodynamics of Bodies in Coning Motion," *AIAA Journal*, Vol. 10, No. 11, 1972, pp. 1517 – 1522.

Weinacht, P., "Navier-Stokes Predictions of Pitch Damping for Axisymmetric Projectiles," *J. of Spacecraft and Rocket*, Vol. 34, No. 6, 1997, pp. 753-761.

Weinacht, P., Guidos, B.J., Sturek, W.B., and Hodes, B.A., "PNS Computations for Spinning Shell at Moderate Angles of Attack and for Long L/D Finned Projectiles," BRL-MR-3522, Ballistic Research Laboratories, Aberdeen Proving Ground, MD, June 1986.